Lab on a Chip

View Online
Dynamic Article Links

Cite this: *Lab Chip*, 2011, **11**, 2167

www.rsc.org/loc

PAPER

Multiplex digital PCR: breaking the one target per color barrier of quantitative PCR†

Qun Zhong,[a] Smiti Bhattacharya,[a] Steven Kotsopoulos,[a] Jeff Olson,[a] Valérie Taly,[b] Andrew D. Griffiths,[b] Darren R. Link[a] and Jonathan W. Larson*[a]

Received 13th February 2011, Accepted 20th April 2011
DOI: 10.1039/c1lc20126c

Quantitative polymerase chain reactions (qPCR) based on real-time PCR constitute a powerful and sensitive method for the analysis of nucleic acids. However, in qPCR, the ability to multiplex targets using differently colored fluorescent probes is typically limited to 4-fold by the spectral overlap of the fluorophores. Furthermore, multiplexing qPCR assays requires expensive instrumentation and most often lengthy assay development cycles. Digital PCR (dPCR), which is based on the amplification of single target DNA molecules in many separate reactions, is an attractive alternative to qPCR. Here we report a novel and easy method for multiplexing dPCR in picolitre droplets within emulsions—generated and read out in microfluidic devices—that takes advantage of both the very high numbers of reactions possible within emulsions (>10^6) as well as the high likelihood that the amplification of only a single target DNA molecule will initiate within each droplet. By varying the concentration of different fluorogenic probes of the same color, it is possible to identify the different probes on the basis of fluorescence intensity. Adding multiple colors increases the number of possible reactions geometrically, rather than linearly as with qPCR. Accurate and precise copy numbers of up to sixteen per cell were measured using a model system. A 5-plex assay for spinal muscular atrophy was demonstrated with just two fluorophores to simultaneously measure the copy number of two genes (SMN1 and SMN2) and to genotype a single nucleotide polymorphism (c.815A>G, SMN1). Results of a pilot study with SMA patients are presented.

Introduction

The advent of PCR and real-time PCR methodologies has greatly improved the analysis of nucleic acids from both throughput and quantitative perspectives. While traditional PCR techniques[1] typically rely on end-point, and sometimes semi-quantitative, analysis of amplified DNA targets *via* agarose gel electrophoresis, quantitative real-time PCR (qPCR) methods are geared toward accurately quantifying exponential amplification as the reaction progresses. qPCR reactions are monitored either using a variety of highly sequence specific fluorescent probe technologies, or by using non-specific DNA intercalating fluorogenic dyes.

As the need for higher throughput in analyzing multiple targets in parallel continues to escalate in the fields of genomics and genetics, and as the need for more efficient use of sample grows in medically related fields such as diagnostics, the ability to perform and quantify multiple amplifications simultaneously within the same reaction volume (multiplexing) is paramount for both PCR and qPCR. While end-point PCR can support a high level of amplicon multiplexing,[2] such ample capacity for multiplexing probe-based qPCR reactions remains elusive for a number of reasons. For example, most commercial real-time thermal cyclers only support up to four differently colored fluorophores for detection as a consequence of the limited spectral resolution of common fluorophores, translating into a multiplexing capacity of 4×. Additionally, while optimization of single target primer/probe reactions is now standard practice, combining primers and probes for multiple reactions changes the thermodynamic efficiencies and/or chemical kinetics, necessitating potentially extensive troubleshooting and optimization. Very high multiplexing of >100× has been demonstrated in a "one of many" detection format for pathogen identification using "sloppy" molecular beacons and melting points as fingerprints, however the approach is restricted to applications with a slim likelihood of the presence of multiple simultaneous targets.[3] A half-multiplexing method achieved 19× in a two step reaction with general multiplexed preamplification in the first step, followed by separate single-plex quantitative PCR in the

[a]*RainDance Technologies, Inc., 44 Hartwell Ave., Lexington, MA, 02150, USA. E-mail: larsonj@raindancetech.com*
[b]*Institut de Science et d'Ingénierie Supramoléculaires (ISIS), Université de Strasbourg, CNRS UMR 7006, 8 allée Gaspard Monge, BP 70028, F-67083 Strasbourg Cedex, France*

† Electronic supplementary information (ESI) available. See DOI: 10.1039/c1lc20126c

second step.[4] However a general purpose single-pot solution to qPCR multiplexing does not yet exist.

Digital PCR (dPCR) is an alternative quantitation method in which dilute samples are divided into many separate reactions. The distribution of target DNA molecules among the reactions follows Poisson statistics, and at so called terminal dilution the vast majority of reactions contain either one or zero target DNA molecules.[5–7] Ideally, the number of PCR positive reactions (PCR(+)) equals the number of template molecules originally present. The principle advantage of dPCR compared to qPCR is that it avoids any need to interpret the time dependence of fluorescence intensity—an analog signal—along with the main underlying uncertainty of non-exponential amplification during early cycles. dPCR has been utilized mostly in challenging studies involving minority targets amidst complicated backgrounds such as allelic imbalance and rare mutations in cancer.[8]

Ideally, the sensitivity of dPCR is limited only by the number of independent amplifications that can be analyzed, which has motivated the development of several ultra-high throughput miniaturized methods allowing millions of single molecule PCR reactions to be performed in parallel (discussed in detail elsewhere[9]). In this, and the accompanying manuscript,[10] dPCR was performed in aqueous droplets separated by oil using a microfluidics system.[11–14] Microfluidic approaches allow the rapid generation of large numbers ($>10^6$) of very uniformly sized microdroplets[15] that function as picolitre volume reaction vessels (see reviews of droplet-based microfluidics[16,17]).

In the accompanying manuscript,[10] duplex dPCR in $>10^6$ picolitre volume droplets was demonstrated using two TaqMan® probes, one specific for the mutant and the other for the wild-type DNA, which generate green and red fluorescent signals, respectively. After thermal cycling, the ratio of mutant to wild-type genes was determined by counting the ratio of green to red droplets. This digital procedure allowed the determination of mutant allelic specific imbalance (MASI) in several cancer cell lines and the precise quantification of a mutated *KRAS* oncogene in the presence of a 200 000-fold excess of unmutated *KRAS* genes in genomic DNA. The sensitivity was, therefore, much higher than conventional, bulk, TaqMan® assays using the same probes, which typically cannot detect less than ~1% mutant *KRAS* in a background of non-mutated DNA from normal cells.[18]

In this report we demonstrate a novel strategy for multiplexed dPCR assays that promises much higher multiplexing than possible with existing qPCR or dPCR techniques. It is based on the singular nature of amplifications at terminal dilution that arises because only a single target allele is typically present in any one droplet even when multiple primers/probes targeting different alleles are present. This alleviates the complications that otherwise plague simultaneous competing reactions, such as varying arrival time into the exponential stage and unintended interactions between primers. As will be shown, reactions within microfluidic droplets yield very uniform fluorescence intensity at the end point, and ultimately the intensity depends on the efficiency of probe hydrolysis. Thus, different reactions with different efficiencies can be discriminated on the basis of end point fluorescence intensity alone even if they have the same color. Furthermore, it will also be shown that the efficiencies can be tuned simply by adjusting the probe concentration, resulting in an easy-to-use and general purpose method for multiplexing. We have demonstrated a 5-plex TaqMan® dPCR assay that worked "right out of the box", in contrast to lengthy optimizations that typify qPCR multiplexing to this degree. Adding multiple colors increases the number of possible reactions geometrically, rather than linearly as with qPCR, because individual reactions can be labeled with multiple fluorophores. In the demonstration shown here, two fluorophores (VIC and FAM) were used to distinguish five different reactions.

Spinal muscular atrophy (SMA) was selected for the example demonstration assay due to both its important clinical significance as well as its complicated genetics. It is the second-most prevalent fatal neurodegenerative disease and affects ~1 in 10 000 live births.[19] SMA is most often caused by homozygous absence of exon 7 within the survival of motor neuron 1 gene (SMN1, reviewed by Wirth *et al.*[20]), however the severity of the condition is modulated by the number of gene copies of SMN2 with prognosis ranging from lethal to asymptomatic over 1–5 copy numbers (reviewed by Elsheikh *et al.*[21]). Hence accurate quantitation of SMN2 copy number is important for clinical prognosis and genetic counseling. Aside from large deletions of SMN1, a number of single point mutations or short deletions/duplications within the same gene also account for ~4% of cases of SMA.[22] In a significant step toward a comprehensive SMA assay, the multiplexed dPCR assay demonstrated here contains both copy number assays (for SMN1 and 2) and an assay for one of the prevalent SNPs (c.815A>G).[22]

Results and discussion

Validation of digital PCR performance

Digital PCR performance in the emulsion format was validated by measuring a serial dilution of a reference gene, branched chain keto acid dehydrogenase E1 (BCKDHA). Mixtures of the PCR master mix, 1× primers and probe for BCKDHA, and varying concentrations of a mixture of human genomic DNA (1 : 1 NA14091 and NA13705) were compartmentalized into over one million 5.3 pL droplets in a water-in-fluorinated oil emulsion using the droplet generation microfluidic chip. The emulsion was thermally cycled off-chip and afterwards the fluorescence of each droplet was analyzed in the readout chip (see Fig. 1). In a serial dilution the average number of target DNA molecules per droplet—called the "occupancy" from this point forward—should decrease in direct proportion to the DNA concentration. The occupancy was calculated from Poisson statistics as

$$\text{occupancy} = \ln\left(\frac{P+N}{N}\right), \quad (1)$$

where P and N are the numbers of PCR(+) and PCR(−) droplets respectively (see derivation in the ESI†).

Droplets were analyzed by fluorescence while flowing through the readout chip to count the numbers of PCR(+) and PCR(−) droplets (see Fig. 1c). As each droplet passed the detection zone (marked with an arrow in Fig. 1c), a burst of fluorescence was observed. To account for small run-to-run differences in the fluorescence intensity that can occur due to different chip positioning, *etc.*, each set of data was scaled such that the average fluorescence intensity of the empty droplets was 0.1 V. Fig. 2a

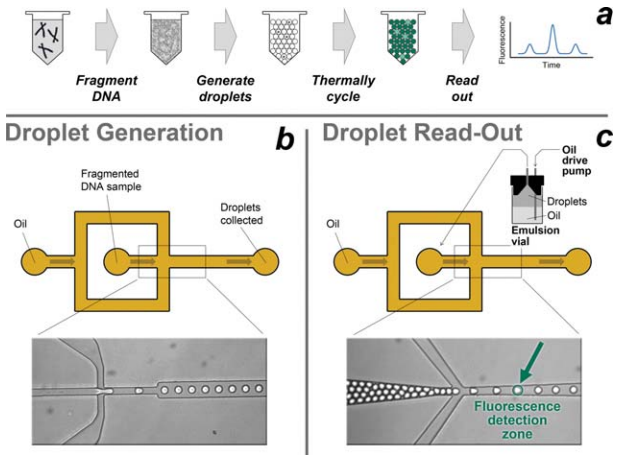

Fig. 1 System diagram of sample preparation, droplet generation, and assay readout. (a) Overview of operations. (b) Droplet generation. A continuous aqueous phase containing fragmented genomic DNA, the PCR master mix, primers, and probes was injected into the fluidic intersection from the left, and the carrier oil entered from the top and bottom. An emerging bolus of aqueous liquid was imaged inside the intersection just prior to snapping off into a discrete droplet as the fluidic strain began to exceed the surface tension of the aqueous liquid. The steady train of droplets leaving the intersection toward the right was collected directly *via* PEEK tubing into a PCR tube and then thermally cycled. The DNA concentration was sufficiently dilute such that the majority of droplets contained either zero or one target DNA molecules. During thermal cycling, only those droplets containing target DNA molecules would increase in fluorescence due to cleavage of the TaqMan® probes during target amplification. (c) Droplet readout. The thermally cycled emulsion was loaded into a custom transfer vial, consisting of a glass body with a molded plastic cap. Once loaded with sample, the vial was connected directly to the readout chip. The oil drained from the emulsion during off-chip handling, hence the emulsion appeared tightly packed in the image before the intersection. The oil introduced in the intersection separated the droplets before sequential readout by laser-induced fluorescence at the location marked by the green arrow.

shows a very short duration of a typical trace of fluorescence bursts from individual droplets for the sample with the highest DNA concentration in the series. PCR(+) and PCR(−) droplets were easily discriminated by fluorescence intensity. The two large bursts of fluorescence peaking at ~0.8 V arose from the PCR(+) droplets, whereas the smaller bursts due to incomplete fluorescence quenching in the PCR(−) droplets peaked at ~0.1 V. A histogram of peak intensities from the complete data set revealed two clear populations centered at 0.10 and 0.78 V (Fig. 2b), demonstrating that the trend evident in the short trace in Fig. 2a was stable over much longer periods of time. Integration over the two populations in Fig. 2b yielded a total of 197 507 PCR(+) and 1 240 126 PCR(−) droplets. Hence the occupancy was 0.15 for this sample by eqn (1), corresponding to the expected occupancy of 0.18 based on the measured DNA concentration of 110 ng μL^{-1}. The occupancy was measured for each sample in the serial dilution and fit to the dilution equation (Fig. 2c):

$$\text{occupancy}(n) = \frac{A}{f^n}, \qquad (2)$$

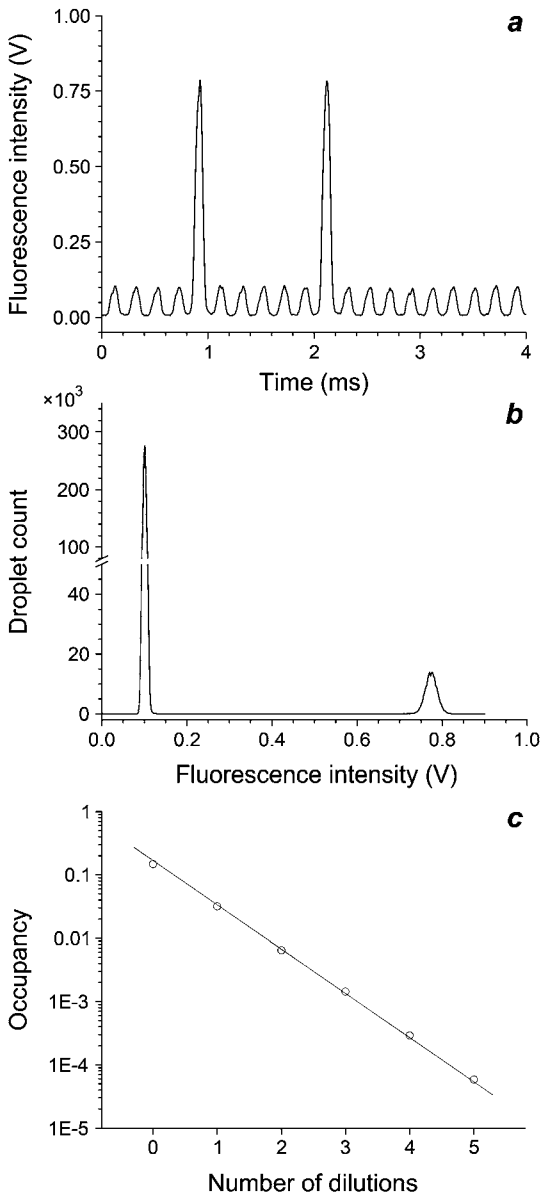

Fig. 2 Serial dilution of template DNA quantified by dPCR. (a) Droplet fluorescence during readout for the most concentrated sample. Each discrete burst of fluorescence corresponded to an individual droplet. Two different groups of droplets were evident: PCR(+) droplets peaking at ~0.8 V and PCR(−) droplets at ~0.1 V. (b) Histogram of the peak fluorescence intensities of droplets from the complete data trace in (a). PCR(+) and PCR(−) droplets appeared as two very distinct populations centered at 0.78 and 0.10 V respectively. (c) Serial dilution of template DNA. Open circles: measured occupancies; solid line: the best fit to eqn (2) ($A = 0.15$, $f = 4.8$, $R^2 = 0.9999$).

where n is the number of dilutions, A is the occupancy at the starting concentration ($n = 0$), and f is the dilution factor. The linear fit was in excellent agreement with the data, with an R^2 value of 0.9999 and the fitted dilution factor of 4.8 in close agreement with the expected value of 5.0.

Monochromatic gene copy number assay

Accurate measurements of gene copy number were obtained by dPCR using probes with the same fluorophore (FAM) for both

the reference and the target DNA. A model system was used with varying concentrations of plasmid DNA to represent a change in the target gene copy number, relative to a reference gene, equivalent to 0–16 copies of the target gene per cell. BCKDHA and SMN2 plasmid DNA served as the reference and target with 1× and 0.5× primers and probes respectively. With a starting ratio of 8 : 1 SMN2 to BCKDHA, the sample was diluted serially by 2× into a solution of BCKDHA at the same concentration to vary just the amount of SMN2. The resultant samples were emulsified, thermally cycled, and over 10^5 droplets were analyzed for each sample as described in the previous section. The process was repeated in triplicate.

To identify fluorescence signatures unique to each probe, histograms of the droplet fluorescence intensities are shown in Fig. 3a for three different template DNA samples: a no template control (dotted green line), BCKDHA only (solid red line), and 1 : 1 BCKDHA to SMN2 (dashed blue line). For clarity, the histograms are shown both overlapped to highlight the similarity for certain peaks, and offset from each other to reveal all of the features. In the case of 1 : 1 BCKDHA to SMN2, three populations were readily apparent: a dominant feature appeared at 0.08 V, and two smaller peaks were evident at 0.27 and 0.71 V. The dominant feature at 0.08 V was assigned to PCR(−) droplets since both small peaks disappeared, but the large one remained, in the no template control. The peak at 0.71 V was assigned to BCKDHA since it was the sole feature arising with the addition of just BCKDHA, and the peak at 0.27 V appeared on subsequent addition of SMN2, completing the assignments. A very small peak appeared at ~0.9 V, not visible on the scale of Fig. 3a, that corresponded to droplets occupied by both genes. Using the peak assignments, droplets were counted corresponding to each possible state (PCR(+) for either BCKDHA or SMN2, or both, or PCR(−)), and the gene copy number was then determined from the ratio of occupancies derived using eqn (1). Gene copy numbers were calculated from occupancies, as opposed to directly from the perhaps more intuitive number of droplet counts within each peak, to account for those droplets that may contain multiple target DNA molecules. Gene copy numbers for each sample in the serial dilution are plotted in Fig. 3b against expected values, with an excellent linear fit across the full range ($R^2 = 0.9997$, slope = 1.01), demonstrating accurate and precise measurement of the equivalent of 0 to 16 copies of SMN2 per cell.

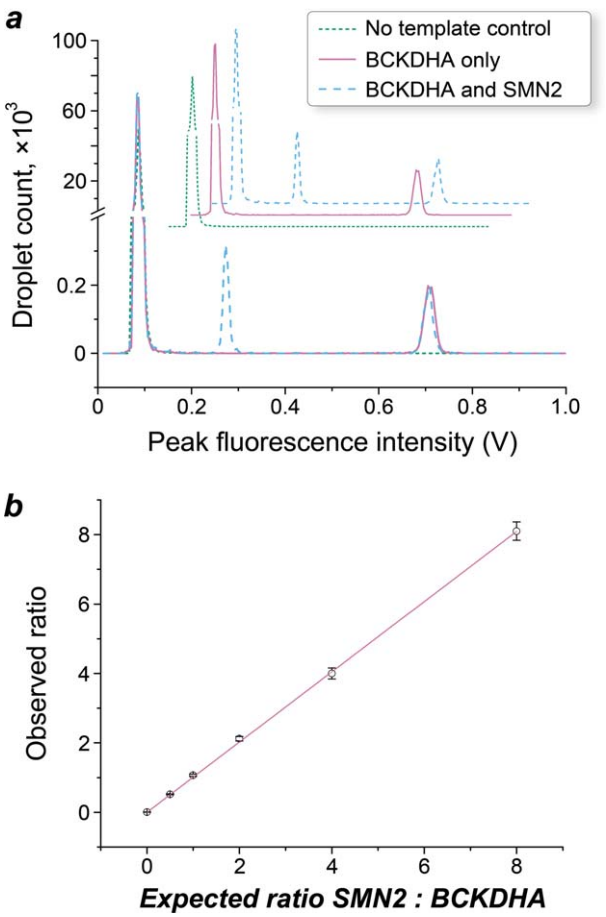

Fig. 3 Duplex gene copy number assay with only one type of fluorophore by dPCR. (a) Histograms of droplet peak fluorescence intensities. For clarity, the histograms are plotted twice, once overlapped showing the high similarity, and again offset from each other toward the upper right to reveal all of the features. Dotted green line: the no template control sample revealed the position of the empty droplets at 0.08 V. Solid red line: the sample with BCKDHA introduced a second peak at 0.71 V. Dashed blue line: the sample with SMN2 and BCKDHA produced a third peak at ~0.27 V. In summary, from left to right, three clear populations of droplets were evident: PCR(−), SMN2(+), and BCKDHA(+). (b) Comparison of gene copy numbers measured by monochromatic dPCR, as observed ratios of SMN2 to BCKDHA to expected ratios of SMN2 to BCKDHA. Line, best linear fit ($y = 1.01x$, $R^2 = 0.9997$).

Tuning TaqMan® probe fluorescence intensity

Identifying probes by fluorescence intensity begets a need for adjusting the brightness of the probes, particularly for higher-plex assays with dense probe patterns. In the previous section the probes for the gene copy number assay yielded very well resolved peaks (Fig. 3a). Clearly room exists to accommodate one or multiple extra probes in the copy number assay within the resolution of the measurement, but a method for adjusting the fluorescence intensity of the new probes is required to avoid interference with the existing assay. We varied the probe and primer concentrations together as a very simple method to optimize relative intensities in higher-plex reactions. Fig. 4 shows probe fluorescence intensities throughout a serial dilution of the probes and primers for a different reference gene, ribonuclease P (RNaseP), against a constant amount of genomic DNA from the Coriell cell line NA3814 at an occupancy of 0.02 target DNA molecules per droplet. The probe fluorescent intensities varied in direct proportion to probe concentration over a narrow concentration range spanning ~0.15 to 0.4 μM ($R^2 = 0.995$)—roughly centered about the typical probe concentration of 0.2 μM—after compensation for dilution errors and other run-to-run differences such as optical realignments using the intensity of the PCR(−) droplets as a reference. In summary, probe intensities can be varied by dilution over a small but adequate range for the purpose of tuning multiplexed assays without affecting the amplification itself.

Higher-plex reactions

A 5-plex assay was demonstrated for common genetic variants impacting SMA including two copy number assays for the

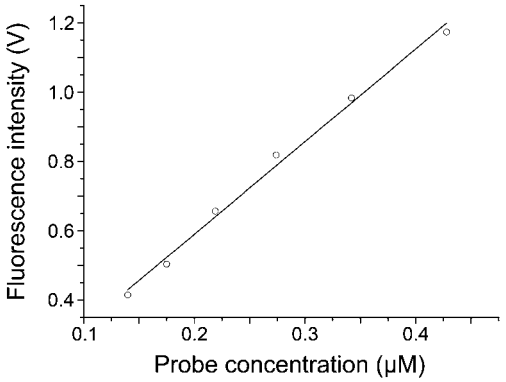

Fig. 4 Linear dependence of droplet fluorescence intensity on probe concentration. Line, best linear fit ($y = -0.092x + 0.082$, $R^2 = 0.995$).

SMN1 and SMN2 genes with BCKDHA as a reference, and a SNP assay for the c.815A>G mutation. Two differently colored fluorophores, FAM and VIC, were used to uniquely identify each of the assays. The probes for SMN1 and SMN2 contained only FAM, and for c.815A only VIC. However, mixtures of VIC and FAM-labeled probes were used for BCKDHA and c.815G. For validating the assay, a model chromosome was synthesized containing a single target region for each of the different primer/probe pairs. EcoRV restriction sites flanked each target, allowing separation of the fragments.

Fig. 5a shows a 2-dimensional histogram of droplet fluorescence intensities as a heat map, with hotter colors representing higher occurrences. Standard techniques were used to compensate for spectral overlap of the FAM and VIC signals. Samples were run at 0.006 occupancy per target. Six populations were clearly evident, five for the assay and one for PCR(−) droplets. The populations were assigned by selective exclusion of assay components. For example, excluding the SMN2 primers and probe eliminated the population at the bottom right in the histogram, but otherwise the distribution remained unchanged. Assignments are labeled in Fig. 5a. As we have found to be generally true for this method of multiplexing, the assay worked immediately with well resolved or at least distinguishable populations for each target. The relative positions of the different populations in the histogram were then adjusted into a regularly spaced rectangular array by tuning the probe concentration as described in the previous section. Usually no more than two iterations are required for optimization.

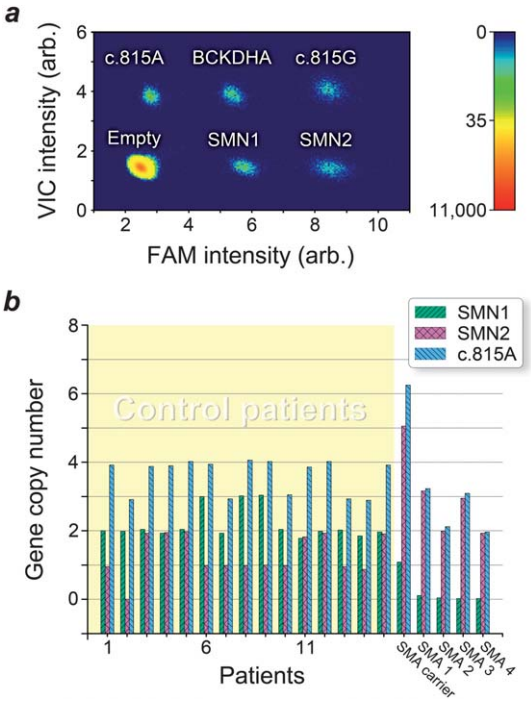

Fig. 5 5-Plex dPCR assay for spinal muscular atrophy with only two fluorophores. (a) 2D histogram of droplet fluorescence intensities, shown as a heat map, for the 5-plex assay against the synthetic model chromosome for validation. The six well resolved droplet populations corresponded to the five individual assays plus the empty droplets. (b) Results of the SMA pilot study.

The different populations were sufficiently well resolved to allow droplets within each population to be counted by integration across rectangular boundaries. The boundaries were positioned at mid-sections between neighboring peaks. The peak position of each cluster varied by no more than 2% from run to run after normalization to the intensity of the empty droplets to account for variations in detection efficiency (data not shown). Hence, once identified, the same boundaries for integration could be reused between samples. Twenty different patient samples from the Coriell cell repositories were analyzed with this assay: 4 afflicted with SMA, 1 SMA carrier, and 15 negative controls. Assay results are shown in Fig. 5b. Gene copy number was calculated as before, as the ratio of occupancies derived from the number of target droplets *vs.* reference droplets. Like the copy number measurement in Fig. 3, each assay yielded ratios very close to the expected integer values, but when all of the patient data was plotted as actual ratio *vs.* expected integer ratio a small systematic deviation from the ideal slope of 1 was observed. Measured slopes were 0.92, 0.92, and 0.99 for SMN1, SMN2, and c.815A respectively. For clarity, the data in Fig. 5b were scaled to the ideal slope of 1.

The measured genotypes of the different patients were consistent with their disease conditions (unafflicted, carrier, or afflicted). The patients afflicted with SMA each had zero copies of SMN1 (numbers SMA 1–4 in Fig. 5b), the carrier had just one copy, and the negative controls all had two or three copies (numbers 1–15). Three unrelated individuals (numbers 6, 8, and 9) had three copies of SMN1, occurring at a rate of 20% which is similar to a previous report for healthy individuals.[23] Variability in SMN1 copy number is not surprising since it lies within an unstable region of chromosome 5q13.[24] A larger variety of SMN2 copy numbers was observed. One to two copies were most common in the control group, although one individual had zero copies, a distribution consistent with expectations for normal individuals.[23] The SMA carrier and afflicted patients had elevated copy numbers of SMN2 on average: 5 for the carrier, two afflicted with 3 copies, and the others with 2 copies. The afflicted patients were all diagnosed as SMA Type I, the most severe form, based on clinical observations according to the Coriell repository. The strong genotype/phenotype correlation between SMN2 copy number and disease severity suggests that the two individuals with three copies of SMN2 might have an improved Type II prognosis, especially for the patient SMA 1

who had survived to three years at the time of sampling, much beyond the typical maximum life expectancy for SMA Type I of 2 years. However there remains reluctance to predict disease outcome based on SMN2 copies alone since other less well characterized or unknown modifying genes may impact prognosis and because not all SMN2 copies may be complete genes.[21] Furthermore some Type I patients have begun surviving longer in newer clinical settings.[21] Hence, with little clinical information regarding the patients available to us, we can conclude that our SMN2 assay results were consistent with broad expectations for disease severity.

The SNP assay revealed that all patients carried the normal c.815A genotype and no instances of c.815G were observed. The mutation is relatively rare and hence was not expected to appear in a small patient panel. Of interest, however, was the presence of an apparent extra gene fragment in two unrelated individuals that was uncovered with the SNP assay. The c.815A>G assay does not discriminate between SMN1 and SMN2 due to their high sequence similarity, and hence the total copies of c.815A and G should equal the sum of the copies of SMN1 and SMN2. This was true for all patients except for healthy patients number 1 and 2, both of whom had one extra copy of c.815A. c.815 lies on exon 6, and the SNP that discriminates between the SMN1 and SMN2 genes lies on exon 7, hence the extra genes may be fragments of SMN1 lacking exon 7. This seems reasonable because the deletion of exon 7 is the common mutation causing 95% of cases of SMA (reviewed by Wirth *et al.*[20]) and it is carried by 1/40 to 1/60 adults.[25] Thus these patients might have been typical carriers of SMA but for the acquisition of at least one compensating healthy copy of SMN1 on the same chromosome.

Multiplexing capacity

The level of multiplexing demonstrated in this report (5×) already reaches the maximum practicable number with qPCR, however higher multiplexing should be readily achievable with dPCR by optimal spacing of the fluorescence intensities of different assays. The two main limitations are the resolution between assays and the increasing fluorescence intensity of empty droplets with higher loading of probes. With the excellent resolution of the different assays shown in the SMA multiplex (Fig. 5a), it is conservative to extrapolate that at least one more row and column of assays could be added for a total multiplexing of >10×. We have achieved a 10× assay by this approach with little difficulty (data not shown). Adding extra colors would increase the capability even further, however with some diminishing returns because the fluorescence of the empty droplets would continue to rise. The capacity could be yet further increased with better probes yielding larger differential signals, such as hybrid 5′-nuclease/molecular beacon probes that reduce background by contact quenching yet exhibit the bright signals typical of free unquenched fluorophores.[26] With such improvements multiplexing capacity exceeding 50× can be envisioned.

Using droplet-based microfluidics, multiple targets can also be assayed in a single experiment in a different way: in the accompanying manuscript the six common mutations in *KRAS* codon 12 were screened in parallel in a single experiment by one-to-one fusion of drops containing genomic DNA with any one of seven different types of droplets, each containing a TaqMan® probe specific for a different *KRAS* mutation, or wild-type *KRAS*, and an optical code.[10] Within the limits imposed by the spectral overlap of fluorophores, both the droplet fusion approach and the multiplex approach described herein can be combined to analyze large numbers of target genes in a single experiment, likely leading to future applications with greater than 100× multiplexing.

Experimental

Primers and probes

All TaqMan® primers and probes used in this study are listed in Table 1. Unless otherwise noted by reference in the table, the primers and probes were designed with the "Custom TaqMan® Assay Design Tool" from Applied Biosystems Inc. (ABI) and procured through ABI (Carlsbad, CA). Probes were labeled with 6-carboxyfluorescein (FAM, λ_{ex} 494 nm\$\lambda_{em}$ 522 nm) or VIC™ (from ABI, λ_{ex} 528 nm\$\lambda_{em}$ 554 nm).

Target DNA

For some genetic targets, BCKDHA and SMN2, plasmid DNA was synthesized (GeneArt, Regensburg, Germany) containing the sequence spanning between the primers (see Table 1) and cloned into the GeneArt standard vector (2.5 kb). The target fragment was released from the cloning vector by restriction digestion with SfiI to avoid any DNA supercoiling that might affect the assay. For simplicity, these gene fragments are called "plasmid DNA" throughout the text. A string of different gene fragments was also synthesized (GeneArt) and cloned into the GeneArt standard vector for demonstration of multiplexed reactions, called an "artificial chromosome" in the text. In this case, the fragments were separated from each other by restriction digestion at flanking EcoRV sites. Human DNA was obtained in already purified form from cell lines (see ESI Table S1†; Coriell, Camden, NJ) and fragmented before use with a K7025-05 nebulizer following manufacturer's instructions (Invitrogen, Carlsbad, CA). DNA concentration was quantified by measuring absorbance at 260 nm on a Nanodrop 2000 spectrophotometer (Thermo Scientific, Wilmington, DE).

Microfluidics

Microfluidic chips were manufactured by conventional soft lithography.[27] Molding masters were fabricated by spin coating SU-8 negative photoresist (MicroChem Corp., Newton, MA) onto 6 inch silicon wafers and transferring the fluidic features from photomasks (CAD/Art Services, Bandon, OR) by contact lithography with an OAI Hybralign Series 200 aligner (OAI, San Jose, CA). Chips contained channels with two depths: deep channels with low hydrodynamic resistance (100 ± 10 μm) for transporting fluid from external ports to the functional regions of the chip, and shallow channels (20 ± 1 μm) for droplet manipulation and detection. SU-8 photoresists 2100 and 2025 were used for deep and shallow channels respectively. Polydimethylsiloxane (PDMS) (Sylgard® 184, Dow Corning, Midland, MI) chips were molded from the negative masters

Table 1 5′-Exonuclease genotyping assay design. Assay conditions in column 5 are specific to the multiplexed SMA assay. "MGBNFQ" is the minor groove binder non-fluorescent quencher

Target	Assay	Primers (5′ to 3′)	Probe (5′ to 3′)	5-Plex assay conditions	Ref.
SMN1	Copy number	(f) AATGCTTTTTAACAT CCATATAAAGCT (r) CCTTAATTTAAGGA ATGTGAGCACC	FAM–CAGGGTT TC*AGACAAA–MGBNFQ	0.37×	28
SMN2	Copy number	(f) AATGCTTTTTAACA TCCATATAAAGCT (r) CCTTAATTTAAGGA ATGTGAGCACC	FAM–TGATTTTGTCT A*AAACCC–MGBNFQ	0.76×	28
BCKDHA	Copy number	(f) CAACCTACTCTTCT CAGACGTGTA (r) TCGAAGTGATCC AGTGGGTAGTG	(FAM/VIC)–CAGGAGA TGCCCGC CCAGCTC–TAMRA	FAM: 0.18× VIC: 0.56×	29
c.815A>G	SNP	(f) TGCTGATGCTTTGG GAAGTATGTTA (r) TGTCAGGAAAAGA TGCTGAGTGATT	(A) VIC–CATGAGTGGCTA*TCATAC–MGBNFQ (G) FAM–ATGAGTGGCTG*TCATAC–MGBNFQ; VIC–CATGAGTGGCTG*TCATAC–MGBNFQ	0.9× FAM: 0.9× VIC: 0.45×	
RNaseP	Copy number	Unknown	Unknown	n/a	Standard product, 4403326, ABI

within mold housings of custom design. Glass cover slides were permanently bonded to the fluidic side of the chips by surface activation in an AutoGlow™ oxygen plasma system (Glow Research, Phoenix, AZ) followed by immediate contact bonding. To create hydrophobic surfaces, the microfluidic channels as well as the fluid-exposed surfaces of the emulsion vials (see Fig. 1) were treated for ~2 min with 1*H*,1*H*,2*H*,2*H*-perfluorodecyltrichlorosilane (Alfa Aesar, Ward Hill, MA) dissolved in FC-3283 (3M Specialty Materials, St Paul, MN) prepared as a mixture of 18 g silane in 100 μL solvent.

Two different microfluidic devices were used, one for droplet generation and the other for fluorescence readout after thermal cycling. The droplet generation chip created an emulsion of uniformly sized aqueous droplets of template DNA and PCR master mix that was suspended in an inert fluorinated oil with an emulsion stabilizing surfactant, called "carrier oil" within the text (REB carrier oil; RainDance Technologies, Lexington, MA). Droplets were generated in a cross-shaped microfluidic intersection, or "nozzle".[15] As shown in Fig. 1c, under typical operation the aqueous phase flowed into the nozzle from the left (160 μL h^{-1}), joining flows of the carrier oil from the top and bottom (750 μL h^{-1} of total oil), and producing 4 pL droplets at a rate of 11 kHz. The channel widths at the intersection measured 15 μm for the aqueous inlet, 12.5 for the oil inlets, and 15 μm widening to 40 μm at the outlet. Flow was driven by custom OEM pumps (IDEX Corporation, Northbrook, IL).

Approximately 25 μL of the PCR reaction mixture was collected as an emulsion from the droplet generation chip and thermally cycled in a DNA Engine (Bio-Rad, Hercules, CA). The reaction mixture contained 1× TaqMan® universal PCR master mix (Applied Biosystems, Carlsbad, CA), 0.2 mM dNTP (Takara Bio, Madison, WI), and various amounts of primer pairs and probes as described in the results. 1× assay concentration is defined as 0.2 μM probes with 0.9 μM primers. In all cases, when varied from the 1× concentration, the primers and probes were varied by the same amount. The cycler program included a 10 min hot start at 95 °C, and 45 cycles of 15 s at 95 °C and 60 s at 60 °C.

The droplets became concentrated during off-chip handling because the carrier oil is more dense than the aqueous phase and drained down from the emulsion. Hence the droplets were reinjected into the readout chip as a tightly packed emulsion that required dilution prior to readout to properly distinguish one droplet from another. A "spacer" nozzle similar to the droplet generation nozzle above was used to inject uniform plugs of extra carrier oil between droplets immediately before readout. As shown in Fig. 1c, the droplet entrance into the nozzle tapered down into a constriction about the size of an individual droplet forcing the droplets to enter the nozzle in single file and consequently at a stable rate. Opposed flow of the carrier oil from the top and bottom channels separated the droplets uniformly. The channel leaving the spacer nozzle increased in width along the direction of flow, and the droplets were interrogated by laser induced fluorescence at the location along the channel where the width was smaller than or equal to the droplet diameter (marked with an arrow in Fig. 1c). The nozzle dimensions were 15 μm for the droplet entrance and exit, and 20 μm for the oil lines.

Instrumentation

Fluorescence readout was performed by conventional epifluorescence microscopy with a custom microscope. A 20 mW, 488 nm laser source (Cyan; Picarro, Sunnyvale, CA) was expanded 2× and focused by the objective lens (20×/0.45 NA; Nikon, Japan) onto the microfluidic channel. Two band pass filters discriminated the fluorescence collected through the objective lens: 512/25 nm and 543/22 nm for FAM and VIC fluorophores respectively (Semrock, Rochester, NY). Fluorescence was detected by

two H5784-20 photomultipliers (Hamamatsu, Japan) and was typically recorded at a 200 kHz sampling rate with a USB-6259 data acquisition card (National Instruments, Austin, TX). The data traces were smoothed by a seven-point, second-order Savitzky–Golay algorithm before subsequent analysis. Concurrent with the fluorescence read out, the droplets were imaged through the same objective lens with backside illumination from an 850 nm LED (TSHG6200; Vishay Semiconductors, Shelton, CT), a short pass filter to separate the optical paths for fluorescence detection and imaging, and a Guppy CCD camera (Allied Vision Technologies, Newburyport, MA). Droplets were imaged with short illumination pulses (5–20 μs) to avoid image streaking.

Data analysis

Data were analyzed with custom LabView software (National Instruments, Austin, TX) that interpreted droplet events as contiguous bursts of fluorescence intensity above a threshold value. The signal-to-noise ratio was generally quite high and the signal levels were consistent from day to day, hence a fixed threshold value of 50 mV was used predominantly, otherwise the threshold was set by eye. The peak fluorescence intensity was recorded for each droplet event for both VIC and FAM fluorophores. Some coalescence of droplets did occur during thermal cycling, typically as isolated events between two intact droplets forming "doublets." Doublets and the rare larger coalesced events were easily filtered from the data set based on the duration of the fluorescence burst.

Conclusion

We have introduced a new method for multiplexing dPCR with droplet-based microfluidics that takes advantage of the millions of independent reactions possible in emulsions plus the biochemical simplicity of single reactions within individual droplets. The result was an accurate and precise multiplexed measurement of gene copy number across four different targets (and one reference). This multiplexing method should be general for all targets compatible with the TaqMan® assay, as shown here, and also general for all types of fluorogenic assay chemistries such as molecular beacons and Solaris® probes. The combination of high precision, high accuracy, and unprecedented multiplexing capability demonstrated here, plus the high sensitivity demonstrated in the accompanying manuscript,[10] makes dPCR superior to qPCR for many important applications such as copy number variation, expression analysis, and the detection of rare mutants.

References

1 J. M. Bartlett and D. Stirling, *Methods Mol. Biol.*, 2003, **226**, 3–6.
2 A. P. Shuber, L. A. Michalowsky, G. S. Nass, J. Skoletsky, L. M. Hire, S. K. Kotsopoulos, M. F. Phipps, D. M. Barberio and K. W. Klinger, *Hum. Mol. Genet.*, 1997, **6**, 337–347.
3 S. Chakravorty, B. Aladegbami, M. Burday, M. Levi, S. A. Marras, D. Shah, H. H. El-Hajj, F. R. Kramer and D. Alland, *J. Clin. Microbiol.*, 2010, **48**, 258–267.
4 S. Therianos, M. Zhu, E. Pyun and P. D. Coleman, *Am. J. Pathol.*, 2004, **164**, 795–806.
5 P. J. Sykes, S. H. Neoh, M. J. Brisco, E. Hughes, J. Condon and A. A. Morley, *BioTechniques*, 1992, **13**, 444–449.
6 O. Kalinina, I. Lebedeva, J. Brown and J. Silver, *Nucleic Acids Res.*, 1997, **25**, 1999–2004.
7 B. Vogelstein and K. W. Kinzler, *Proc. Natl. Acad. Sci. U. S. A.*, 1999, **96**, 9236–9241.
8 G. Pohl and le.-M. Shih, *Expert Rev. Mol. Diagn.*, 2004, **4**, 41–47.
9 C. Zhang and D. Xing, *Chem. Rev.*, 2010, **110**, 4910–4947.
10 D. Pekin, Y. Skhiri, J.-C. Baret, D. Le Corre, L. Mazutis, C. Ben Salem, F. Millot, A. El Harrak, P. Laurent-Puig, A. D. Griffiths and V. Taly, *Lab Chip*, DOI: 10.1039/c1lc20128j.
11 N. R. Beer, B. J. Hindson, E. K. Wheeler, S. B. Hall, K. A. Rose, I. M. Kennedy and B. W. Colston, *Anal. Chem.*, 2007, **79**, 8471–8475.
12 M. M. Kiss, L. Ortoleva-Donnelly, N. R. Beer, J. Warner, C. G. Bailey, B. W. Colston, J. M. Rothberg, D. R. Link and J. H. Leamon, *Anal. Chem.*, 2008, **80**, 8975–8981.
13 J. Pipper, M. Inoue, L. F. Ng, P. Neuzil, Y. Zhang and L. Novak, *Nat. Med.*, 2007, **13**, 1259–1263.
14 Y. Schaerli, R. C. Wootton, T. Robinson, V. Stein, C. Dunsby, M. A. Neil, P. M. French, A. J. Demello, C. Abell and F. Hollfelder, *Anal. Chem.*, 2009, **81**, 302–306.
15 S. L. Anna, N. Bontoux and H. A. Stone, *Appl. Phys. Lett.*, 2003, **82**, 364.
16 S.-Y. Teh, R. Lin, L.-H. Hung and A. P. Lee, *Lab Chip*, 2008, **8**, 198–220.
17 A. B. Theberge, F. Courtois, Y. Schaerli, M. Fischlechner, C. Abell, F. Hollfelder and W. T. S. Huck, *Angew. Chem., Int. Ed.*, 2010, **49**, 5846–5868.
18 A. Lievre, J. B. Bachet, V. Boige, A. Cayre, D. Le Corre, E. Buc, M. Ychou, O. Bouche, B. Landi, C. Louvet, T. Andre, F. Bibeau, M. D. Diebold, P. Rougier, M. Ducreux, G. Tomasic, J. F. Emile, F. Penault-Llorca and P. Laurent-Puig, *J. Clin. Oncol.*, 2008, **26**, 374–379.
19 J. Pearn, *J. Med. Genet.*, 1978, **15**, 409–413.
20 B. Wirth, M. Herz, A. Wetter, S. Moskau, E. Hahnen, S. Rudnik-Schöneborn, T. Wienker and K. Zerres, *Am. J. Hum. Genet.*, 1999, **64**, 1340–1356.
21 B. Elsheikh, T. Prior, X. Zhang, R. Miller, S. J. Kolb, D. Moore, W. Bradley, R. Barohn, W. Bryan, D. Gelinas, S. Iannaccone, R. Leshner, J. R. Mendell, M. Mendoza, B. Russman, S. Smith, W. King and J. T. Kissel, *Muscle Nerve*, 2009, **40**, 652–656.
22 L. Alías, S. Bernal, P. Fuentes-Prior, M. J. Barceló, E. Also, R. Martínez-Hernández, F. J. Rodríguez-Alvarez, Y. Martín, E. Aller, E. Grau, A. Peciña, G. Antiñolo, E. Galán, A. L. Rosa, M. Fernández-Burriel, S. Borrego, J. M. Millán, C. Hernández-Chico, M. Baiget and E. F. Tizzano, *Hum. Genet.*, 2009, **125**, 29–39.
23 P. E. McAndrew, D. W. Parsons, L. R. Simard, C. Rochette, P. N. Ray, J. R. Mendell, T. W. Prior and A. H. M. Burghes, *Am. J. Hum. Genet.*, 1997, **60**, 1411–1422.
24 S. Lefebvre, L. Bürglen, S. Reboullet, O. Clermont, P. Burlet, L. Viollet, B. Benichou, C. Cruaud, P. Millasseau, M. Zeviani, D. Le Paslier, J. Frézal, D. Cohen, J. Weissenbach, A. Munnich and J. Melki, *Cell*, 1995, **80**, 155–165.
25 J. Melki, S. Lefebvre, L. Burglen, P. Burlet, O. Clermont, P. Millasseau, S. Reboullet, B. Bénichou, M. Zeviani, D. Le Paslier, D. Cohen, J. Weissenbach and A. Munnich, *Science*, 1994, **264**, 1474–1477.
26 D.-M. Kong, L. Gu, H.-X. Shen and H.-F. Mi, *Chem. Commun.*, 2002, 854–855.
27 G. M. Whitesides, E. Ostuni, S. Takayama, X. Jiang and D. E. Ingber, *Annu. Rev. Biomed. Eng.*, 2001, **3**, 335–373.
28 D. Anhuf, T. Eggermann, S. Rudnik-Schöneborn and K. Zerres, *Hum. Mutat.*, 2003, **22**, 74–78.
29 D. DiMatteo, S. Callahan and E. B. Kmiec, *Exp. Cell Res.*, 2008, **15**, 878–886.

